Advanced Robotics, Vol. 17, No. 2, pp. 131–147 (2003)

Also available online - www.vsppub.com

Full paper

Biped walking pattern generation by a simple three-dimensional inverted pendulum model

SHUUJI KAJITA *, FUMIO KANEHIRO, KENJI KANEKO, KIYOSHI FUJIWARA, KAZUHITO YOKOI and HIROHISA HIRUKAWA

National Institute of Advanced Industrial Science and Technology (AIST), Umezono 1-1-1, Tsukuba Ibaraki 305, Japan

Received 16 April 2002; accepted 31 May 2002

Abstract—For three-dimensional (3D) walking control of a biped robot we analyze the dynamics of a 3D inverted pendulum in which motion is constrained to move along an arbitrarily defined plane. This analysis leads us to a simple linear dynamics, the Three-Dimensional Linear Inverted Pendulum Mode (3D-LIPM). The geometric nature of the trajectories under the 3D-LIPM and a method for walking pattern generation are discussed. A simulation result of a walking control using a 12-d.o.f. biped robot model is also shown.

Keywords: Biped robot; walking robot; dynamic walk; biped locomotion; inverted pendulum.

1. INTRODUCTION

Research on humanoid robots and biped locomotion is currently one of the most exciting topics in the field of robotics and there exist many ongoing projects. Although some of those works have already demonstrated very reliable dynamic biped walking [1, 2], we believe it is still important to understand the theoretical background of biped locomotion.

A lot of research dedicated to biped walking pattern generation can be classified into two categories. The first group uses, precise knowledge of the dynamic parameters of a robot, e.g. mass, location of center of mass and inertia of each link, to prepare walking patterns. Therefore, it mainly relies on the accuracy of the model data [1–4].

On the contrary, the second group uses limited knowledge of dynamics, e.g. location of total center of mass, total angular momentum, etc. Since the controller

*To whom correspondence should be addressed. E-mail: s.kajita@aist.go.jp

knows little about the system structure, this approach greatly relies on a feedback control [5–11].

In this paper we take a standpoint of the second approach and introduce a new model which represents a robot dynamics with limited parameters. The model, the Three-Dimensional Linear Inverted Pendulum Mode (3D-LIPM), is derived from a general 3D inverted pendulum whose motion is constrained to move along an arbitrarily defined plane. It allows a separate controller design for the sagittal (x–z) and the lateral (y–z) motion, and simplifies walking pattern generation a great deal.

2. DERIVATION OF 3D-LIPM

2.1. Motion equation of a 3D inverted pendulum

When a biped robot is supporting its body on one leg, its dominant dynamics can be represented by a single inverted pendulum which connects the supporting foot and the center of mass of the whole robot. Figure 1 depicts such an inverted pendulum consisting of a point mass and a massless telescopic leg. The position of the point mass $\boldsymbol{p} = (x, y, z)$ is uniquely specified by a set of state variables $\boldsymbol{q} = (\theta_r, \theta_p, r)$:

$$x = rS_p, \tag{1}$$

$$y = -rS_r, \tag{2}$$

$$z = rD, \tag{3}$$

$$S_r \equiv \sin\theta_r,\ S_p \equiv \sin\theta_p,\ D \equiv \sqrt{1 - {S_r}^2 - {S_p}^2}.$$

Let (τ_r, τ_p, f) be the actuator torque and force associated with the state variables (θ_r, θ_p, r). With these inputs, the equation of motion of the 3D inverted pendulum in Cartesian coordinates is given as follows:

$$m\begin{pmatrix}\ddot{x}\\ \ddot{y}\\ \ddot{z}\end{pmatrix} = \left(\mathbf{J}^{\mathrm{T}}\right)^{-1}\begin{pmatrix}\tau_r\\ \tau_p\\ f\end{pmatrix} + \begin{pmatrix}0\\ 0\\ -mg\end{pmatrix}, \tag{4}$$

where m is the mass of the pendulum and g is gravity acceleration. The structure of the Jacobian $\mathbf{J}$ is:

$$\mathbf{J} = \frac{\partial \boldsymbol{p}}{\partial \boldsymbol{q}} = \begin{pmatrix}0 & rC_p & S_p\\ -rC_r & 0 & -S_r\\ -rC_rS_r/D & -rC_pS_p/D & D\end{pmatrix}, \tag{5}$$

$$C_r \equiv \cos\theta_r,\ C_p \equiv \cos\theta_p.$$

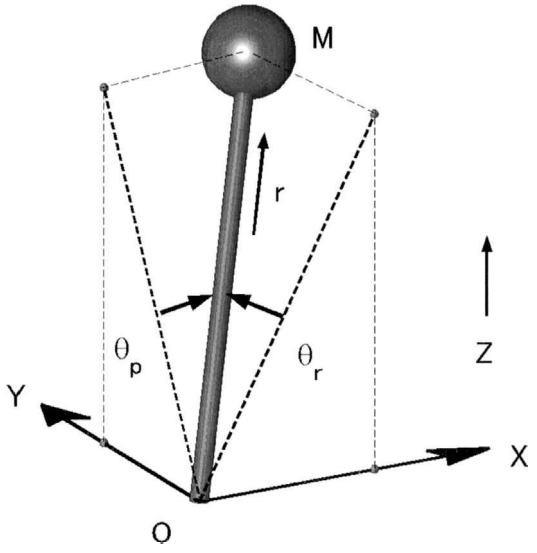

Figure 1. 3D pendulum.

To erase the inversed Jacobian that appears in (4), let us multiply the matrix $\mathbf{J}^{\mathrm{T}}$ from the left:

$$m\begin{pmatrix} 0 & -rC_{\mathrm{r}} & -rC_{\mathrm{r}}S_{\mathrm{r}}/D \\ rC_{\mathrm{p}} & 0 & -rC_{\mathrm{p}}S_{\mathrm{p}}/D \\ S_{\mathrm{p}} & -S_{\mathrm{r}} & D \end{pmatrix}\begin{pmatrix} \ddot{x} \\ \ddot{y} \\ \ddot{z} \end{pmatrix} = \begin{pmatrix} \tau_{\mathrm{r}} \\ \tau_{\mathrm{p}} \\ f \end{pmatrix} - mg\begin{pmatrix} -rC_{\mathrm{r}}S_{\mathrm{r}}/D \\ -rC_{\mathrm{p}}S_{\mathrm{p}}/D \\ D \end{pmatrix}. \tag{6}$$

Using the first row of this equation and multiplying D/C_{r} we get:

$$m(-rD\ddot{y} - rS_{\mathrm{r}}\ddot{z}) = \frac{D}{C_{\mathrm{r}}}\tau_{\mathrm{r}} + rS_{\mathrm{r}}mg. \tag{7}$$

By substituting the kinematic relationship of (2) and (3), we get a good-looking equation that describes the dynamics along the y-axis:

$$m(-z\ddot{y} + y\ddot{z}) = \frac{D}{C_{\mathrm{r}}}\tau_{\mathrm{r}} - mgy. \tag{8}$$

A similar procedure for the second row of (6) yields the equation for the dynamics along the x-axis:

$$m(z\ddot{x} - x\ddot{z}) = \frac{D}{C_{\mathrm{p}}}\tau_{\mathrm{p}} + mgx. \tag{9}$$

2.2. 3D-LIPM

Although the pattern of movement of the pendulum has vast possibilities, we want to select a class of motion that would be suitable for walking. For this reason, we apply constraints to limit the motion of the pendulum. The first constraint limits the motion in a plane with given normal vector $(k_x, k_y, -1)$ and z intersection z_c:

$$z = k_x x + k_y y + z_c. \tag{10}$$

For a robot walking on a rugged terrain, the normal vector should match the slope of the ground and the z intersection should be the expected average distance of the center of the robot's mass from the ground. For further calculation, we prepare the second derivatives of (10):

$$\ddot{z} = k_x \ddot{x} + k_y \ddot{y}. \tag{11}$$

Substituting these constraints into (8) and (9), we obtain the dynamics of the pendulum under the constraints. From straightforward calculations we get:

$$\ddot{y} = \frac{g}{z_c} y - \frac{k_x}{z_c}(x\ddot{y} - \ddot{x}y) - \frac{1}{mz_c} u_r, \tag{12}$$

$$\ddot{x} = \frac{g}{z_c} x + \frac{k_y}{z_c}(x\ddot{y} - \ddot{x}y) + \frac{1}{mz_c} u_p, \tag{13}$$

where u_r, u_p are new virtual inputs which are introduced to compensate for the input non-linearity:

$$\tau_r = \frac{C_r}{D} u_r, \tag{14}$$

$$\tau_p = \frac{C_p}{D} u_p. \tag{15}$$

In the case of the walking on a flat plane, we can set the horizontal constraint plane ($k_x = 0, k_y = 0$) and we obtain:

$$\ddot{y} = \frac{g}{z_c} y - \frac{1}{mz_c} u_r, \tag{16}$$

$$\ddot{x} = \frac{g}{z_c} x + \frac{1}{mz_c} u_p. \tag{17}$$

In the case of walking on a slope or stairs where $k_x, k_y \neq 0$, we need another constraint. From $x\times(12) - y\times(13)$ we see

$$x\ddot{y} - \ddot{x}y = \frac{-1}{mz}(u_r x + u_p y). \tag{18}$$

Therefore, we have the same dynamics of (16) and (17) in the case of an inclined constraint plane by introducing the following new constraint about the inputs:

$$u_r x + u_p y = 0. \tag{19}$$

Equations (16) and (17) are independent linear equations. The only parameter which governs those dynamics is z_c, i.e. the z intersection of the constraint plane, and the inclination of the plane never affects the horizontal motion. Note that the original dynamics were nonlinear and we derived linear dynamics without using any approximation.

We call this the 3D-LIPM. Kajita and Tani introduced a 2D version of this dynamics mode [9] in 1991, and Hara *et al.* extended it to three dimensions in the case of zero input torque [12] in 1997.

3. NATURE OF THE 3D-LIPM

In this section, we examine nature of trajectories under the 3D-LIPM with zero input torques ($u_r = u_p = 0$):

$$\ddot{y} = \frac{g}{z_c} y, \tag{20}$$

$$\ddot{x} = \frac{g}{z_c} x. \tag{21}$$

With a given initial condition, these equations determine a trajectory in 3D space. Figure 2 shows two examples.

3.1. Similarity and difference with gravity field

We can regard that (20) and (21) represent a force field for a unit mass:

$$f = \frac{g}{z_c} r. \tag{22}$$

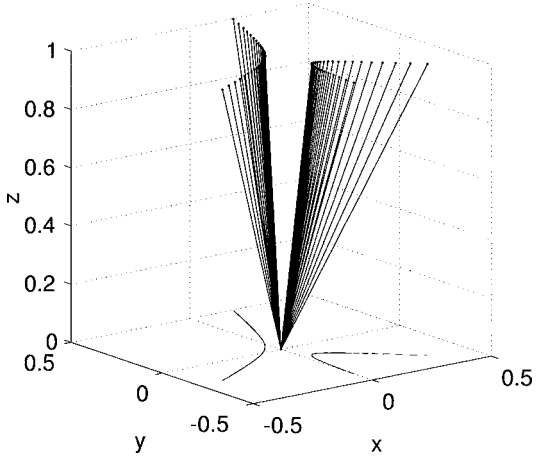

Figure 2. 3D-LIPM.

A unit mass is driven by a force vector of magnitude f that is proportional to the distance r between the mass and the origin. The force magnitude can be distributed into x and y element as follows:

$$f_y = f\left(\frac{y}{r}\right) = \frac{g}{z_c}y, \tag{23}$$

$$f_x = f\left(\frac{x}{r}\right) = \frac{g}{z_c}x. \tag{24}$$

Equation (22) reminds us of the celestial mechanics under the gravity field. In this case, the force magnitude is:

$$f_G = -\frac{k_G}{r^2}, \tag{25}$$

where k_G is a parameter determined from the gravity constant and the mass of the gravity source. Both in (22) and (25), the force vectors are parallel to the position vectors from the origin to the mass. This results in the well-known Kepler's second law of planetary motion: areal velocity conservation.

Let us see how the force of gravity can be separated into x and y direction.

$$f_{Gx} = \frac{x}{r}\left(-\frac{k_G}{r^2}\right) = -\frac{xk_G}{(x^2+y^2)^{3/2}}, \tag{26}$$

$$f_{Gy} = \frac{y}{r}\left(-\frac{k_G}{r^2}\right) = -\frac{yk_G}{(x^2+y^2)^{3/2}}. \tag{27}$$

Since x affects f_{Gy} and y affects f_{Gx}, we must always treat these two equations as a set. On the contrary, the x and y element of the 3D-LIPM can be treated independently at all times. This gives us great advantages in analyzing and in designing walking patterns as we will see in the following sections.

3.2. Geometry of the trajectory

Figure 3 shows a 3D-LIPM trajectory which is projected onto the XY plane. Motions along Y and X are governed by (20) and (21), respectively. By integrating

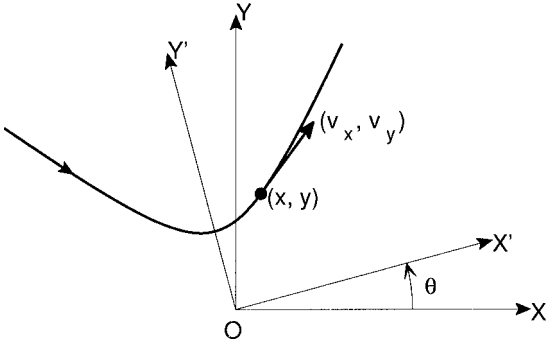

Figure 3. 3D-LIPM projected onto the XY plane.

each equation, we obtain a time-invariant parameter named the *orbital energy* [9]:

$$E_y = -\frac{g}{2z_c}y^2 + \frac{1}{2}\dot{y}^2, \tag{28}$$

$$E_x = -\frac{g}{2z_c}x^2 + \frac{1}{2}\dot{x}^2. \tag{29}$$

Figure 3 shows another coordinate frame $X'Y'$ which rotates θ from the original frame XY. Since the 3D-LIPM is a dynamics under the central force field as discussed in the last section, the new frame $X'Y'$ also gives a proper representation of the 3D-LIPM. The new orbital energy is calculated as

$$E'_x = -\frac{g}{2z_c}(cx + sy)^2 + \frac{1}{2}(c\dot{x} + s\dot{y})^2, \tag{30}$$

$$E'_y = -\frac{g}{2z_c}(-sx + cy)^2 + \frac{1}{2}(-s\dot{x} + c\dot{y})^2, \tag{31}$$

where $c \equiv \cos\theta$, $s \equiv \sin\theta$. By simple calculations we can verify that the total energy of the system does not change by the way of the coordinate setting:

$$E'_x + E'_y = E_x + E_y = \text{constant}. \tag{32}$$

When the Y'-axis corresponds to the axis of symmetry as in Fig. 3, E'_x and E'_y become maximum and minimum, respectively. Therefore, we can calculate the axis of symmetry by solving the following equation:

$$\frac{\partial E'_x}{\partial \theta} = A\left(s^2 - c^2\right) + Bsc = 0, \tag{33}$$

where:

$$A \equiv (g/z_c)xy - \dot{x}\dot{y}, \tag{34}$$

$$B \equiv (g/z_c)\left(x^2 - y^2\right) - \left(\dot{x}^2 - \dot{y}^2\right). \tag{35}$$

The solution is when $B \neq 0$:

$$\theta = \frac{1}{2}\tan^{-1}(2A/B), \tag{36}$$

when $B = 0$, $A \neq 0$:

$$\theta = \pi/4, \tag{37}$$

when $B = 0$, $A = 0$:

$$\theta = \text{atan2}(y, x). \tag{38}$$

If the Y-axis happens to be already the axis of symmetry, θ should be zero. From (36) and (34), the following condition must be satisfied (since $B = 0$ rarely happens, we do not consider (37) and (38)):

$$(g/z_c)xy - \dot{x}\dot{y} = 0. \tag{39}$$

Using this equation, we can calculate the geometric shape of the 3D-LIPM. By substituting (28) and (29):

$$(g/z_c)^2 x^2 y^2 = \dot{x}^2 \dot{y}^2 = \left(2E_x + (g/z_c)x^2\right)\left(2E_y + (g/z_c)y^2\right).$$

The final form is a simple quadratic equation:

$$\frac{g}{2z_c E_x} x^2 + \frac{g}{2z_c E_y} y^2 + 1 = 0. \tag{40}$$

Since $E_x > 0$ and $E_y < 0$, (40) forms a hyperbolic curve.

Hyperbolic curves also appear in Kepler motion and one of the examples is a *swing by flight* of the *Voyager 1* spacecraft approaching Jupiter in 1979 [13]. It seems interesting that we obtained the same shape of trajectory from a totally different potential field.

4. 3D WALKING PATTERN GENERATION

4.1. Outline

Figure 4 shows an example of a walking pattern based on the 3D-LIPM. In this paper we assume support leg exchange of constant pace. To change the walking speed and direction, the robot modifies foot placements (shown as small circles in Fig. 4).

When we project the walking motion on to the X- and Y-axes, we observe decoupled motions governed by (21) and (20) (Fig. 5). Each motion follows the 2D version of the Linear Inverted Pendulum Mode that we described in a previous paper [9].

4.2. Pattern generation along a local axis

Now the problem becomes a control of the motion along the X- or Y-axis for each step. Let us assume that the robot is repeating a single support phase of duration T_s and double support phase of duration T_{dbl}.

Figure 6 illustrates successive steps in the X-direction. The initial body state $(x_i^{(n)}, v_i^{(n)})$ and the final body state $(x_f^{(n)}, v_f^{(n)})$ have the following relationship:

$$\begin{pmatrix} x_f^{(n)} \\ v_f^{(n)} \end{pmatrix} = \begin{pmatrix} C_T & T_c S_T \\ S_T/T_c & C_T \end{pmatrix} \begin{pmatrix} x_i^{(n)} \\ v_i^{(n)} \end{pmatrix}, \tag{41}$$

$$T_c \equiv \sqrt{z_c/g},\ C_T \equiv \cosh(T_s/T_c),\ S_T \equiv \sinh(T_s/T_c).$$

To control the walking speed, we must change the foothold (point E) to modify the initial condition of the support phase (D′ → F). When the desired status at the

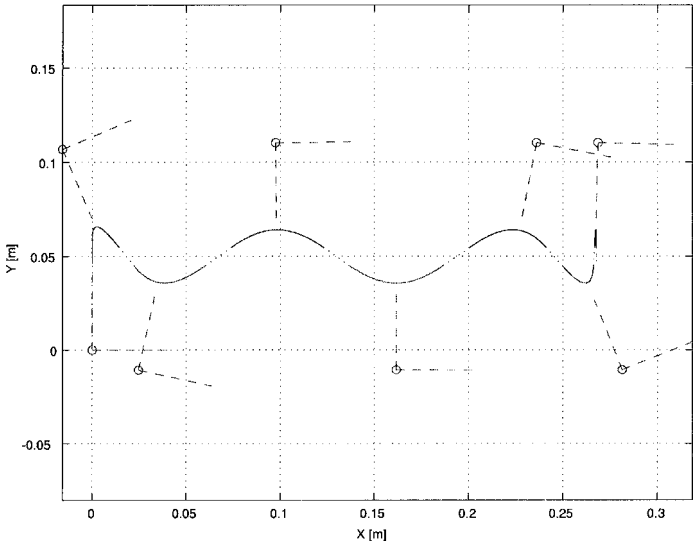

Figure 4. Walking pattern generated from the 3D-LIPM. A robot takes seven steps from left to right. The motion of the tip of the inverted pendulum is shown as pieces of hyperbolic curves (solid lines). We assume that the robot is in double support and moves on a straight line between each support phase (dotted lines). Small circles are foot places and dashed lines indicate primary axes of the hyperbolic curve.

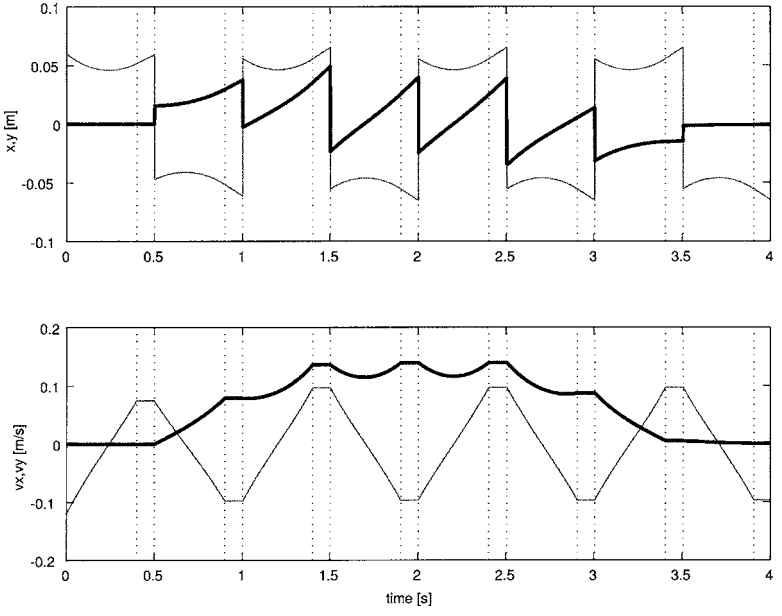

Figure 5. XY position and velocity in the walk in Fig. 4. The thick line shows x motion and the thin line shows y motion. The position graphs jump the distance of the step length at each support foot exchange, since we are taking an origin at a foot place of each support. The vertical dotted lines indicate the time of the supporting mode change. In this walking pattern, the robot takes 0.4 s for single support and 0.1 s for double support.

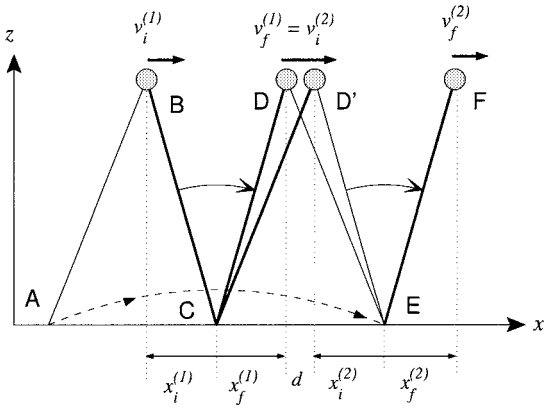

Figure 6. Two successive steps in the sagittal plane are illustrated. The body travels from B to D in the single-leg support phase, then moves from D to D′ in the double-leg support phase with constant speed $v_f^{(1)}$ and then travels from D′ to F in the second single-support phase. While the body moves from B to D, the tip of the swing leg travels from A to E (dashed curved line). By changing the position of E we can control the final body speed $v_f^{(2)}$ at the point F. Except for our inserted double-support phase, this is the same idea proposed by Miura and Shimoyama [14].

end of support (point F) is given as (x_d, v_d) we can define error norm with certain weight $a, b > 0$ as

$$N \equiv a(x_d - x_f^{(2)})^2 + b(v_d - v_f^{(2)})^2.$$

By substituting (41) into this equation and calculating the foothold of $x_i^{(2)}$ which minimizes N, we obtain a proper control law:

$$x_i^{(2)} = (aC_T(x_d - S_T T_c v_f^{(1)}) + bS_T/T_c(v_d - C_T v_f^{(1)}))/D_T, \tag{42}$$

$$D_T \equiv aC_T^2 + b(S_T/T_c)^2.$$

To determine the foothold E, we also need the distance that the body travels in the double support. The distance is

$$d = v_f^{(1)} T_{dbl}. \tag{43}$$

The motion of the swing leg is planned to arrive at the point E at the expected touchdown time (dashed curve from A to E in Fig. 6).

4.3. Control of the walking direction

To specify the walking direction, we rotate the reference XY frame step by step (see Fig. 3). The control of (42) automatically shapes the robot motion to follow the given frame of reference. Figure 7 illustrates walking along a circle. In this

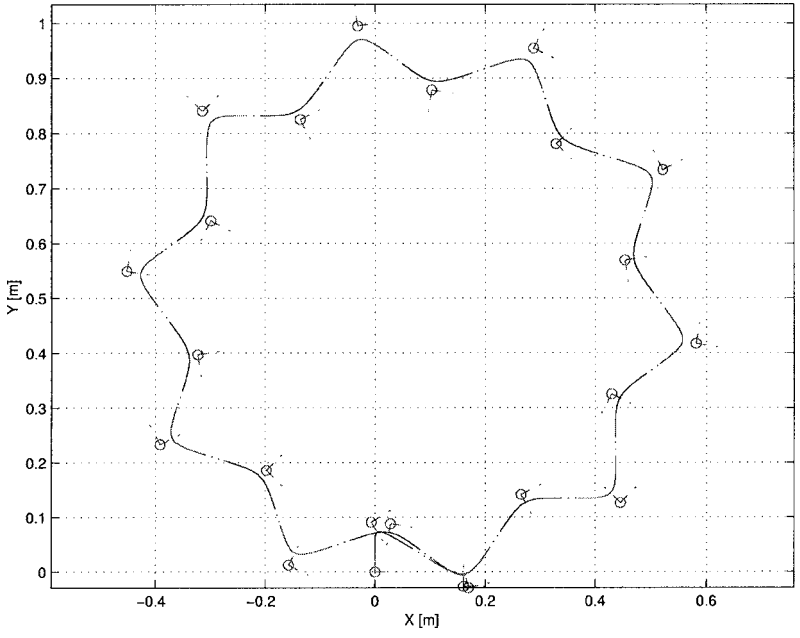

Figure 7. Walk on a circle.

walking pattern, the reference frame is rotated $\pi/10$ rad so that the robot returns to the stating point with 20 steps.

5. SIMULATION OF HUMANOID WALKING

The 3D-LIPM has already been applied to a non-humanoid-type biped robot that has telescopic legs. Although the robot could perform 3D dynamic biped walking without using the prepared trajectory, the walking direction control has not yet been considered [15].

In this paper, we examine a simulated humanoid robot whose motion is generated by the 3D-LIPM. Figure 8 shows the outlook of the robot used in the simulation. The robot has 6 d.o.f. for each leg, but the arms and the head are modeled as one block with the body. Table 1 shows important physical parameters determined by considering an actual mechanical design. The size of the foot is 0.21 m $\times$ 0.1 m (length $\times$ width). The total mass of the robot is 56 kg and the center of mass is located 0.542 m in the height from the floor level.

For the dynamic simulation we used the *OpenHRP simulator* which was developed in METI's humanoid robotics project [16]. The walking pattern of Fig. 7 was used as a reference input to the robot and the center of mass of the robot body was controlled to follow this. To walk on a flat floor, the body height was kept constant. The reference joint angles and speeds were calculated by inverse kinematics so that

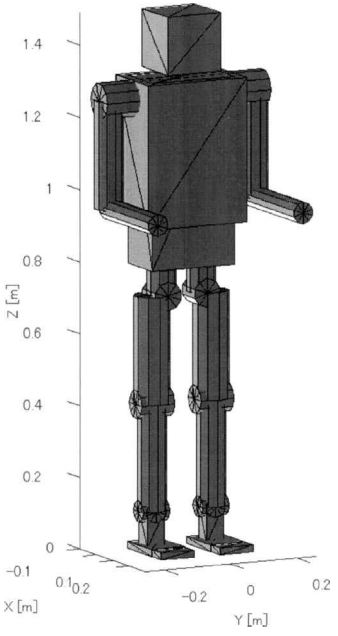

Figure 8. A humanoid robot model. The total mass of the robot is 56 kg and the center of mass is located 0.542 m in the height from the floor level. The robot has 6 d.o.f. for each leg, but the arms and the head do not contain any joints (modeled as one block with the body).

Table 1.
Important link parameters

Length (m)	
width of pelvis[a]	0.12
thigh link	0.3
schank link	0.3
ankle-sole distance	0.11
foot length	0.21
foot width	0.1
Weight (kg)	
body	20
crotch yaw	1
crotch roll	2
thigh	5
shank	4
ankle pitch	3
foot	3
Moment of inertia of the body (kgm^2)	
I_{xx}	0.5548
I_{yy}	0.4882
I_{zz}	0.1417

[a] Distance between the right and left hip joints.

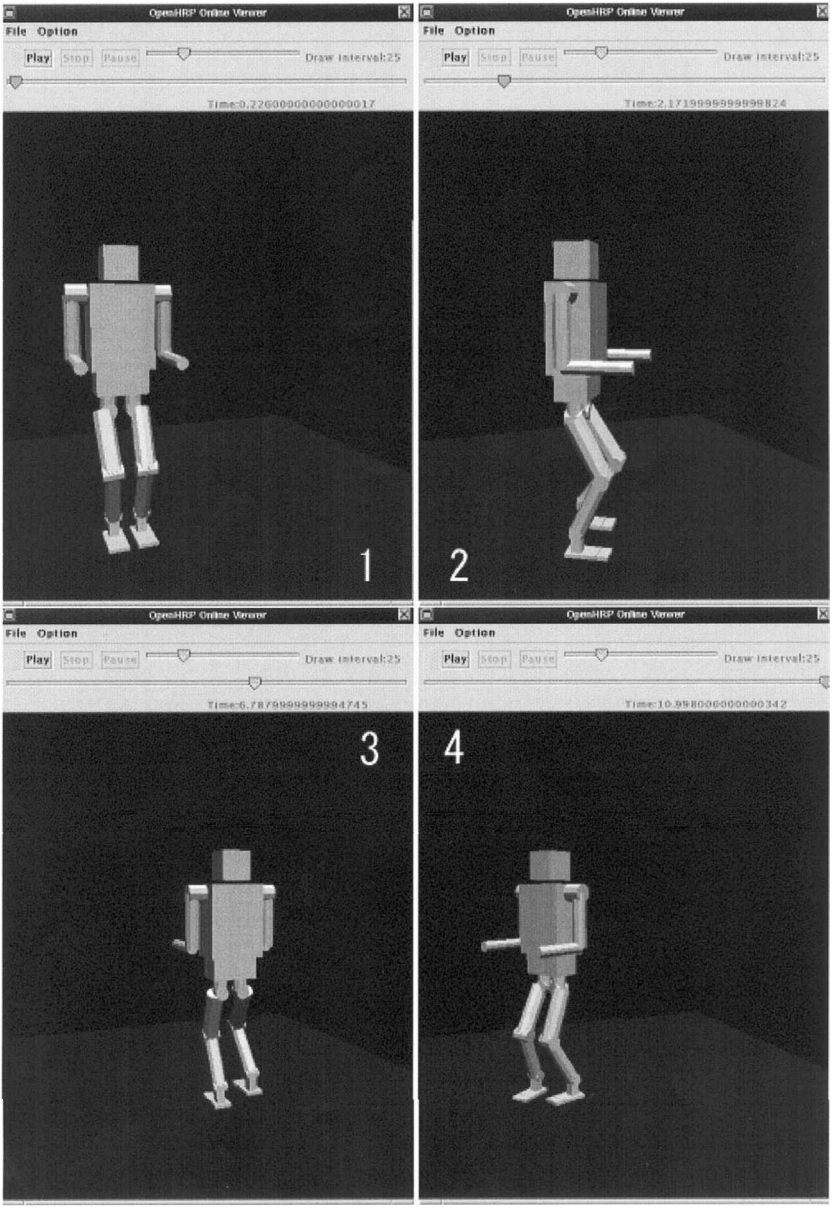

Figure 9. Snapshots of the humanoid simulator.

the position and the velocity of the feet with respect to the body correspond to the specified motion. Finally, the reference joint angles and speeds were realized by a PD feedback controller.

Furthermore, we must consider the body and the foot rotation around the z-axis. Although the walking pattern of Fig. 7 assumes an ideal robot that can step towards

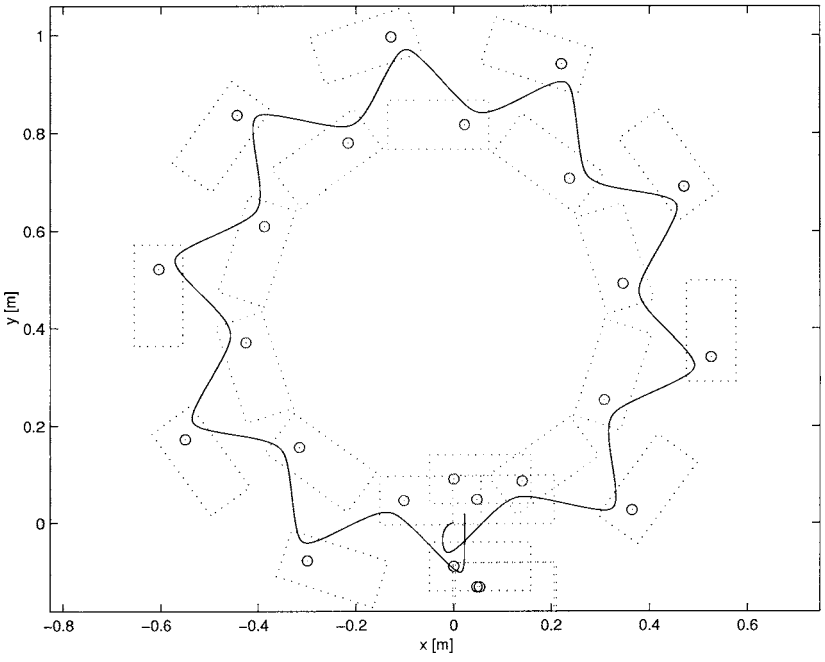

Figure 10. Hip motion and foot placement.

any direction at all times, the robot of Fig. 8 has limited joint angles and it must avoid collisions between the left and the right legs. For this reason we designed additional pattern for the foot orientation with respect to the body, so that the body faces the instantaneous walking direction in the middle of each support.

Figure 9 shows snapshots of the simulation and Fig. 10 shows the body trajectory and foot placements. We can observe the robot returns to the initial position after 20 steps with good accuracy except for a slight difference at the initiation and the termination for the walking sequence.

6. SUMMARY AND CONCLUSIONS

In this paper, we introduced the 3D-LIPM that is useful for walking control in a 3D space. We discussed a nature of the 3D-LIPM and proposed a simple walking pattern generation that can specify walking speed and direction. The walking pattern was tested on a 12 d.o.f. humanoid robot in a dynamic simulator and a dynamically stable walk along a circle was successfully simulated.

Since our method requires a small amount of computation, we can use our pattern generator for the real-time walking control of an actual biped robot. This is reported elsewhere [17].

Acknowledgements

This research was supported by the Humanoid Robotics Project of the Ministry of Economy, Trade and Industry, through the Manufacturing Science and Technology Center.

REFERENCES

1. K. Hirai, M. Hirose, Y. Haikawa and T. Takenaka, The development of Honda humanoid robot, in: *Proc. Int. Conf. on Robotics and Automation*, Leuven, Belgium, pp. 1321–1326 (1998).
2. J. Yamaguchi, E. Soga, S. Inoue and A. Takanishi, Development of a bipedal humanoid robot — control method of whole body cooperative dynamic biped walking, in: *Proc. Int. Conf. on Robotics and Automation*, Detroit, MI, pp. 368–374 (1999).
3. K. Nishiwaki, K. Nagasaka, M. Inaba and H. Inoue, Generation of reactive stepping motion for a humanoid by dynamically stable mixture of pre-designed motions, in: *Proc. Int. Conf. on Systems, Man and Cybernetics*, Tokyo, Japan, no. VI, pp. 702–707 (1999).
4. Q. Huang, S. Kajita *et al.*, A high stability, smooth walking pattern for a biped robot, in: *Proc. Int. Conf. on Robotics and Automation*, Detroit, MI, pp. 65–71 (1999).
5. M. Raibert, *Legged Robots that Balance*. MIT Press, Cambridge, MA (1986).
6. J. Furusho and A. Sano, Sensor-based control of a nine-link biped, *Int. J. Robotics Res.* **9** (2), 83–98 (1990).
7. A. Sano and J. Furusho, Realization of natural dynamic walking using the angular momentum information, in: *Proc. Int. Conf. on Robotics and Automation*, Cincinnati, OH, Vol. 3, pp. 1476–1481 (1990).
8. Y.F. Zheng and J. Shen, Gait synthesis for the SD-2 biped robot to climb sloping surface, *IEEE Trans. Robotics Automat.* **6** (1), 86–96 (1990).
9. S. Kajita and K. Tani, Study of dynamic biped locomotion on rugged terrain, in: *Proc. Int. Conf. on Robotics and Automation*, Sacramento, CA, pp. 1405–1410 (1991).
10. Y. Fujimoto and A. Kawamura, Three dimensional digital simulation and autonomous walking control for eight-axis biped robot, in: *Proc. Int. Conf. on Robotics and Automation*, Sacramento, CA, pp. 2877–2884 (1995).
11. J. Pratt, P. Dilworth and G. Pratt, Virtual model control of a bipedal walking robot, in: *Proc. Int. Conf. on Robotics and Automation*, Albuquerque, NM, pp. 193–198 (1997).
12. K. Hara, R. Yokokawa and K. Sadao, Dynamic control of biped locomotion robot for disturbance on lateral plane, in: *Proc. Japan Society of Mechanical Engineers 72nd Kansai Meet.*, pp. 10-37–10-38 (1997) (in Japanese).
13. Voyager Project Home Page: http://vraptor.jpl.nasa.gov/voyager/voyager.html
14. H. Miura and I. Shimoyama, Dynamic walk of a biped, *Int. J. Robotics Res.* **3** (2), 60–72 (1984).
15. S. Kajita, O. Matsumoto and M. Saigo, Real-time 3D walking pattern generation for a biped robot with telescopic legs, in: *Proc. Int. Conf. on Robotics and Automation*, Seoul, South Korea, pp. 2299–2308 (2001).
16. F. Kanehiro, N. Miyata, S. Kajita, K. Fujiwara, H. Hirukawa, Y. Nakamura, K. Yamane *et al.*, Virtual humanoid robot platform to develop controllers of real humanoid robots without porting, in: *Proc. IROS*, Maui, HI, pp. 1093–1099 (2001).
17. S. Kajita, F. Kanehiro, K. Kaneko, K. Fujiwara, K. Yokoi and H. Hirukawa, A realtime pattern generator for biped walking, in: *Proc. Int. Conf. on Robotics and Automation*, Washington, DC, pp. 31–37 (2002).

ABOUT THE AUTHORS

Shuuji Kajita received his BE, ME and PhD degrees in Control Engineering from Tokyo Institute of Technology in 1983, 1985 and 1996, respectively. In 1985, he joined the Mechanical Engineering Laboratory, Ministry of International Trade and Industry. Meanwhile, he was a Visiting Researcher at California Institute of Technology, 1996–1997. Currently, he is a Senior Researcher at the National Institute of Advanced Industrial Science and Technology (AIST), Tsukuba, Japan, which was reorganized from AIST-MITI in April 2001. His research interests include robotics and control theory. He is a member of Society of Instrument and Control Engineers, Robotics Society of Japan and IEEE (Robotics and Automation Society).

Fumio Kanehiro received his BE, ME and PhD degrees in 1994, 1996 and 1999, respectively, all from the University of Tokyo. He was a Research Fellow of the Japan Society for the Promotion of Science (JSPS) in 1999. He is now a member of the Intelligent Systems Institute at the National Institute of Advanced Industrial Science and Technology, METI, Japan. His research interests include humanoid robots and developmental software systems. He is a member of the Robotics Society of Japan, Japanese Society for Artificial Intelligence, Japan Society for Software Science and Technology and IEEE.

Kenji Kaneko received his BE, ME and PhD degrees in Electrical Engineering from Keio University in 1988, 1990 and 1997, respectively. In 1990, he joined the Mechanical Engineering Laboratory, AIST-MITI, Tsukuba, Japan, as a Researcher. He is currently the Senior Research Scientist of the Humanoid Research Group, Intelligent Systems Institute, National Institute of Advanced Industrial Science and Technology (AIST), Tsukuba Japan, which was reorganized from AIST-METI in April 2001. From September 1995 to February 1996, he was a Visiting Researcher at Carnegie Mellon University. From October 1999 to September 2000, he was a Visiting Researcher at the Laboratoire de Robotique de Paris, CNRS. His research interests include motion control, biped walking control and whole-body control for humanoids.

Kiyoshi Fujiwara received his BE and ME degrees in 1995 and 1997, respectively, all from Tsukuba University. He joined the Electrotechnical Laboratory, AIST-MITI in 1997 at Tsukuba, Japan. He is currently a Researcher of the Humanoid Research Group, Intelligent Systems Institute, National Institute of Advanced Industrial Science and Technology (AIST), Tsukuba, Japan, which was reorganized from AIST-METI in April 2001. His research interests include humanoid robots, medical engineering and the man–machine interface. He is a member of the Robotics Society of Japan.

Kazuhito Yokoi received his BE degree in Mechanical Engineering from Nagoya Institute of Technology in 1984, and his ME and PhD degrees in Mechanical Engineering Science from Tokyo Institute of Technology in 1986 and 1994, respectively. Since 1986, he has been a Researcher, with the Mechanical Engineering Laboratory, AIST-MITI, Tsukuba, Japan. He is currently a Senior Researcher of the Humanoid Research Group, Intelligent Systems Institute, National Institute of Advanced Industrial Science and Technology (AIST), Tsukuba, Japan. From November 1994 to October 1995, he was a Visiting Scholar at the Robotics Labo-

ratory, Computer Science Department, Stanford University. His research interests include humanoids, human-centered robotics and mobile manipulator control. He is a member of the IEEE Robotics and Automation Society, and IEEE Systems, Man and Cybernetics Society.

Hirohisa Hirukawa received his BS, MS and PhD degrees from Kobe University, Kobe, Japan in 1982, 1984 and 1987, respectively. He joined the Electrotechnical Laboratory, AIST-MITI in 1987. He was a Visiting Scholar at Stanford University from 1994 to 1995. He is currently the Scientific Leader of the Humanoid Robotics Group at AIST. His research interests include robot motion planning, computational geometry, computer algebra, distributed robots and humanoid robotics.